

Supplementary Figure Legends

Supplementary Figure 1. Correlation between persistent and past activity in single recordings.

All conventions are identical to Figure 2, but now the data is plotted for each of rat individually. For each recording, black regression lines are obtained using the data from that animal only. Red and blue regression lines are those computed from the cumulative data in Figure 2, overlaid for comparison. Note that only a subset of the five synchronization ranges is shown for each rat; we omit synchronization ranges having fewer than 20 data points, as the corresponding regression plots are unreliable. As with the pooled data, all recordings show a negative correlation between persistent and past activity in synchronized trials.

Supplementary Figure 2. Relationship between initial and persistent “responses” to past activity in the absence of a stimulus.

All conventions are identical to Figure 2, but produced using “phantom” control trials corresponding to randomly chosen times during which there was no stimulus. (a) Within each synchronization range, trials are sorted by the level of past activity w at the time of the “stimulus.” (b, c) Correlations of activity in the initial and persistent periods with prior activity. Unlike with true stimuli, persistent activity does not show a negative correlation with prior activity in synchronized states, indicating that the negative correlation was indeed a result of the stimulus, and not caused by spontaneous up/down transitions. In the most desynchronized states, however (bottom), the positive correlation with prior activity seen in Fig. 2 remains, suggesting that this correlation reflected a return to baseline activity, rather than a true effect of the stimulus. Activity in the initial period also shows a positive correlation with prior activity, due to continuity of the smoothed MUA trace in the absence of a stimulus. (d) Regression slopes for initial and persistent “responses” as a function of synchronization range for control trials.

Supplementary Figure 3. Persistent vs. past activity in control trials for varying τ . To verify that the results of Supplementary Figure 2 are independent of the choice of τ for “phantom” control trials, we repeated the analysis with τ ranging from 20ms to 200ms, in 20ms steps. Each column shows scatterplots for the five synchronization ranges, for the indicated value of τ . In all cases, the regression lines show a similar pattern to that seen in Supplementary Fig. 2. (Differences in “n” values for the same synchronization range are a result of small differences in the number of outliers removed for different τ .)

Supplementary Figure 4. Persistent vs. past activity in control trials for varying τ in rat 1 only.

Same analysis as in Supplementary Fig. 3, but restricted to rat 1; this is the recording that was used to find the optimal value $\tau = 100\text{ms}$ used in Figure 2 (and throughout the paper). As in Supplementary Figure 1 (rat 1), synch range 5 is not shown because there were fewer than 20 data points.

Supplementary Figure 5. Behavior of the deterministic and noise-driven FitzHugh-Nagumo model for various phase portrait topologies.

For deterministic dynamical systems, the qualitative behavior of the system is determined by the topology of the phase portrait, but for noise-driven systems this is not the case. (a) Five different phase portraits obtained for different parameters of the FHN model. The straight line $v=w$ in each is the w -nullcline, while the other curve gives the v -nullcline. Fixed points are color-coded according to whether they are stable (blue), unstable (red), or saddle (green). The arrangement of fixed points and nullclines, including fixed point stability, determines the topology of the phase portrait. The first four phase portraits are topologically distinct, whereas phase portraits 4 and 5 (bottom) have the same topology. (b) Deterministic (blue) and noise-driven (red) trajectories were computed and superimposed on the phase portrait for each model, with initial condition $(0.1,0)$ (green star). The same noise trace was used to generate the stochastic trajectory for each model. (c) Same simulated data as shown in (b), displaying v as a function of time. As expected, deterministic dynamics are sensitive to changes in phase portrait topology, for example changing from oscillatory to non-oscillatory behavior following a shift in fixed point stability. The stochastic (noise-driven) dynamics, on the other hand, show oscillatory behavior for all of the nonlinear models exhibiting a close approach of nullclines (rows 1-4). Conversely, a change from oscillatory to non-oscillatory behavior is seen for the stochastic model between the linear and nonlinear phase portraits shown in rows 4 and 5, even though their topologies are identical and the deterministic dynamics similar.

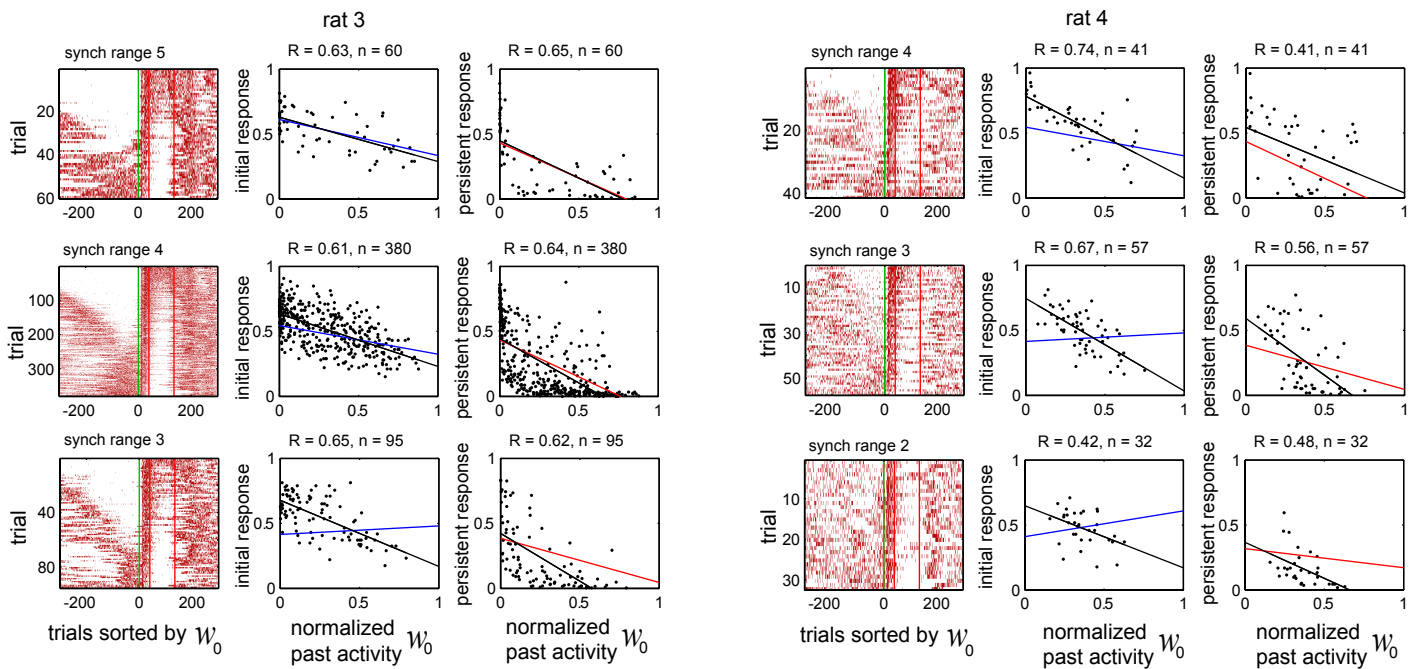
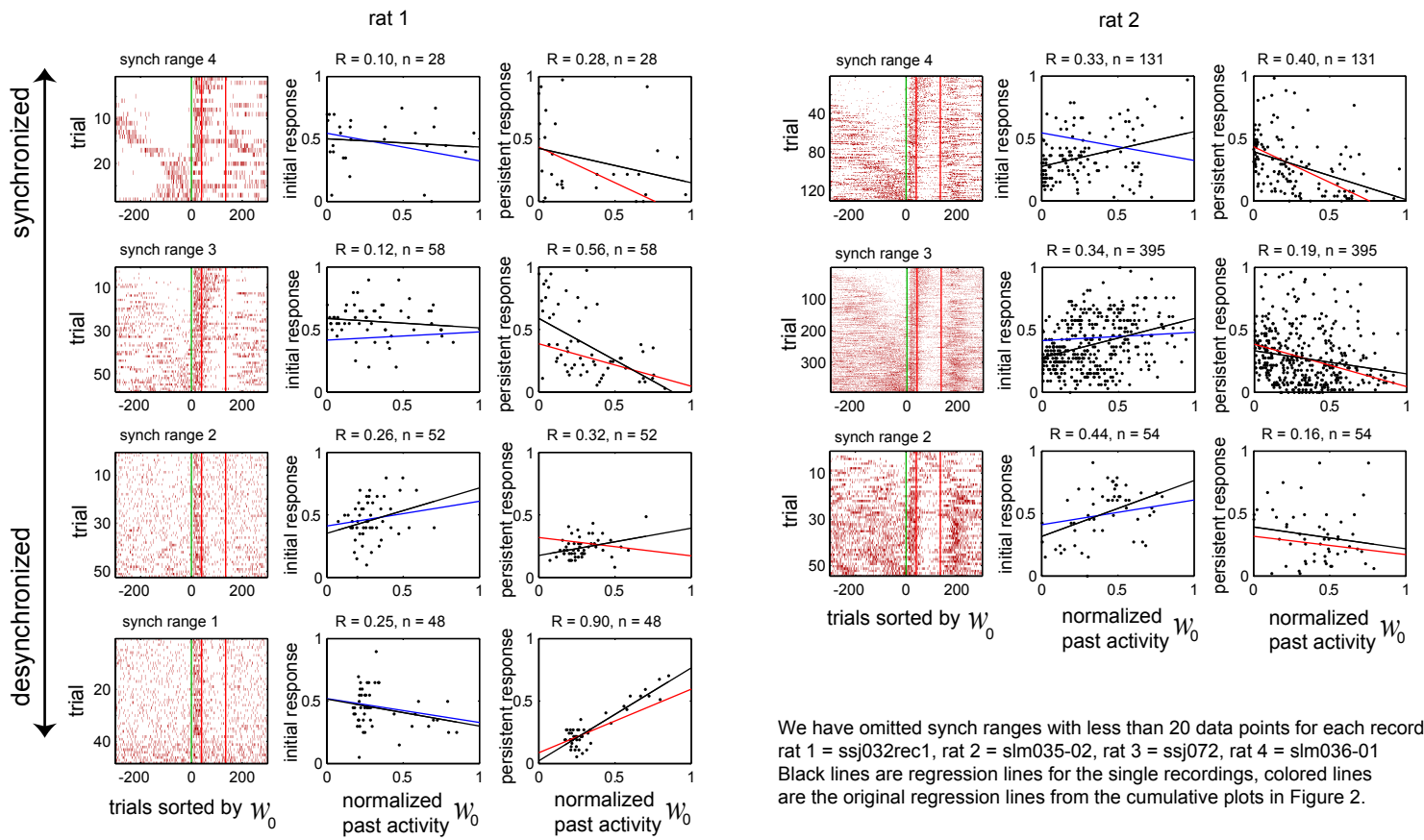
Supplementary Figure 6. Pairwise comparison of model fits between animals.

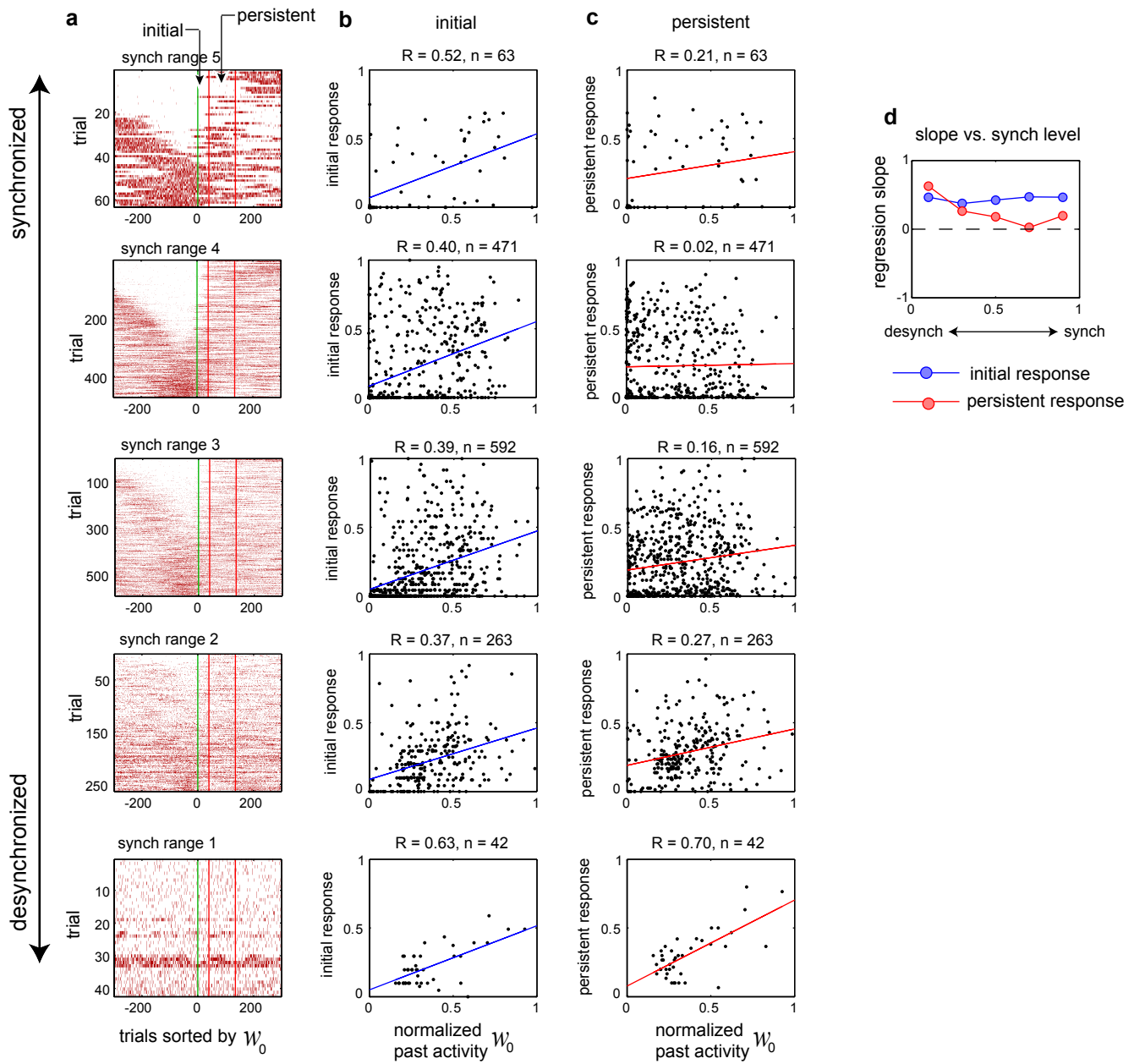
Conventions are the same as in Figure 6e,f, but comparisons are performed pairwise between rats rather than within and across recordings. Percentiles of model performance for each trial in a given rat (denoted on the x-axis) are computed with respect to models obtained from all trials in a comparison rat (separate panels). (a) Comparison model performances on a given trial are computed using both the activity state and dynamic state fit from comparison trials in other recordings. Box plots where the rat number matches the comparison rat are identical to those shown in the “within recording” panel of Figure 6e. Median percentiles (red) are in each case significantly above chance level (50%). (b) Comparison model

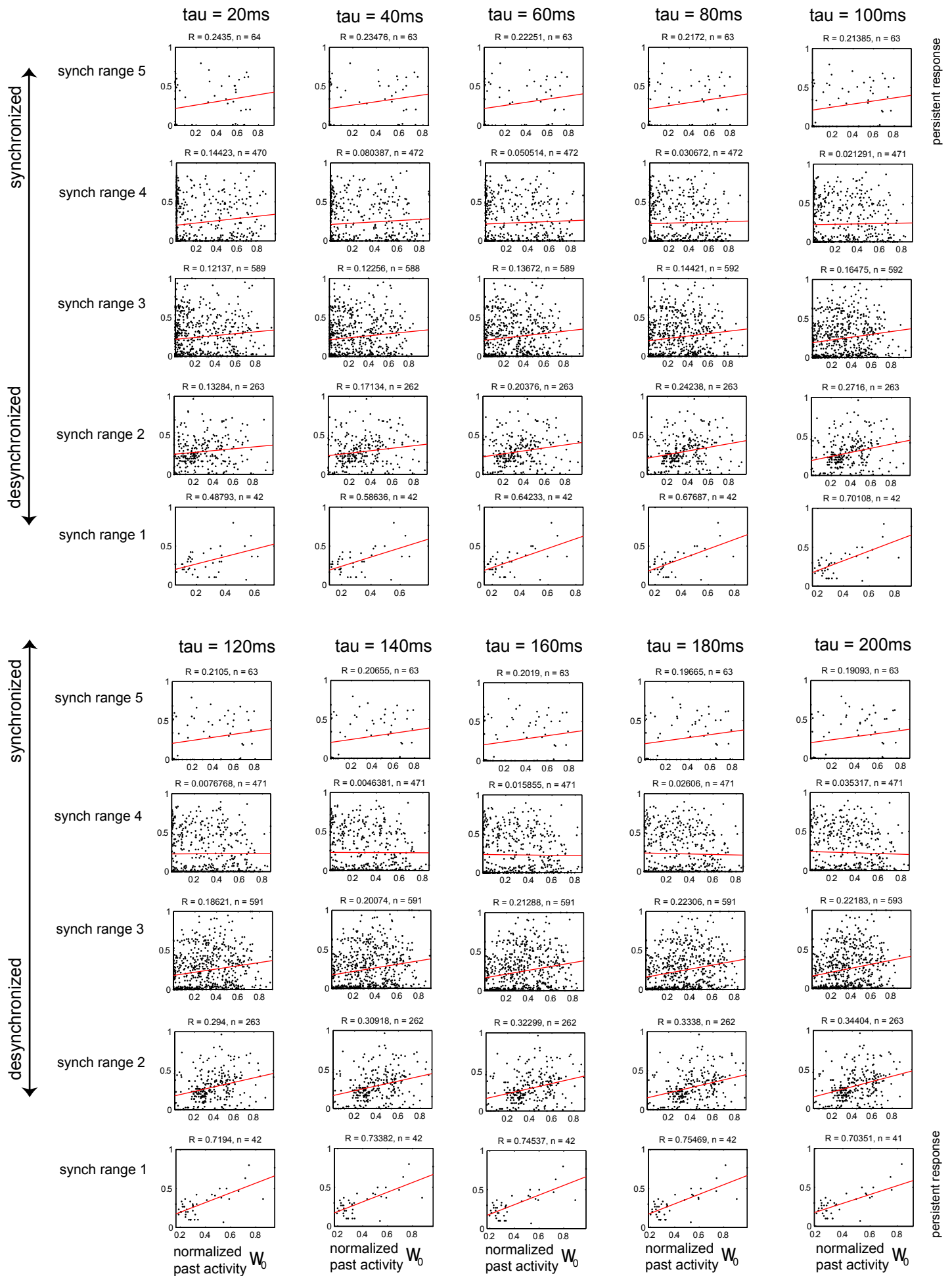
performances on a given trial are computed using only the dynamic state fit from comparison trials in other recordings, and keeping the activity state corresponding to that trial. Box plots where the rat number matches the comparison rat are identical to those shown in the “within recording” of Figure 6f. Median percentiles (red) are significantly above chance level (50%) in all cases except for the “within recording” comparisons for rats 3 and 4 that showed stable dynamic state, consistent with the results of Figure 6f.

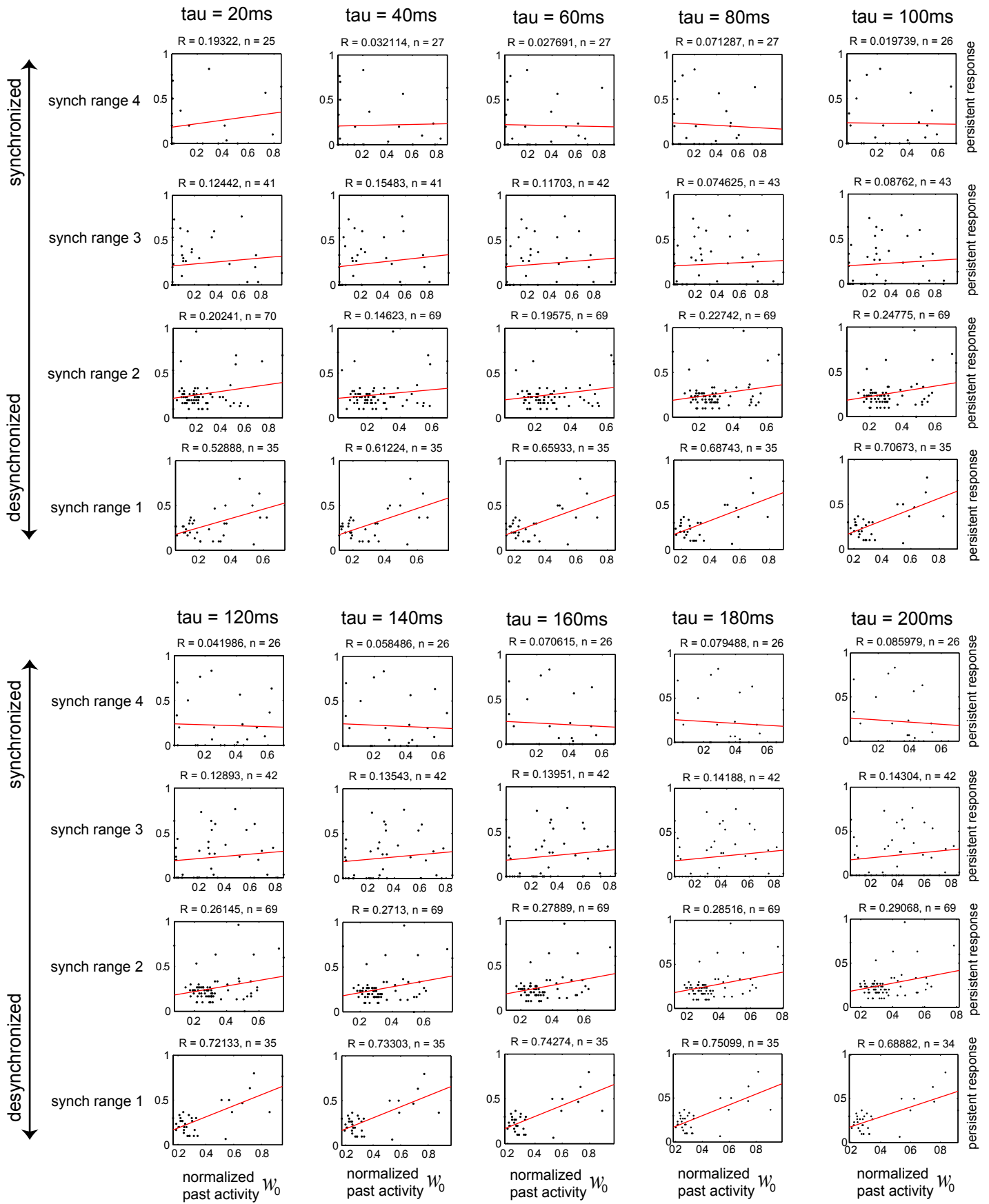
Supplementary Figure 7. PPT stimulation desynchronizes the cortex. (a) LFP (black), units (raster) and smoothed MUA (red) before and after PPT stimulation (pink). Although activity was in the synchronized state preceding PPT stimulation, population activity is highly desynchronized immediately following the stimulation. (b) Desynchronization persists many seconds after PPT stimulation, but gradually returns to synchronized patterns of activity after tens of seconds.

Supplementary Figure 8. Quality of model fits does not correlate with degree of synchronization. Fit error vs. degree of synchronization for each recording (see Methods for definitions of both measures). Each point in the scatterplots corresponds to a single trial, with the fit error computed on the three seconds of data preceding a sensory stimulus. There is no significant correlation between cortical state and the quality of model fits ($p = 0.35, 0.28, 0.35$ and 0.06 on rats 1-4, respectively; $R = 0.07, 0.04, 0.04$ and 0.16).

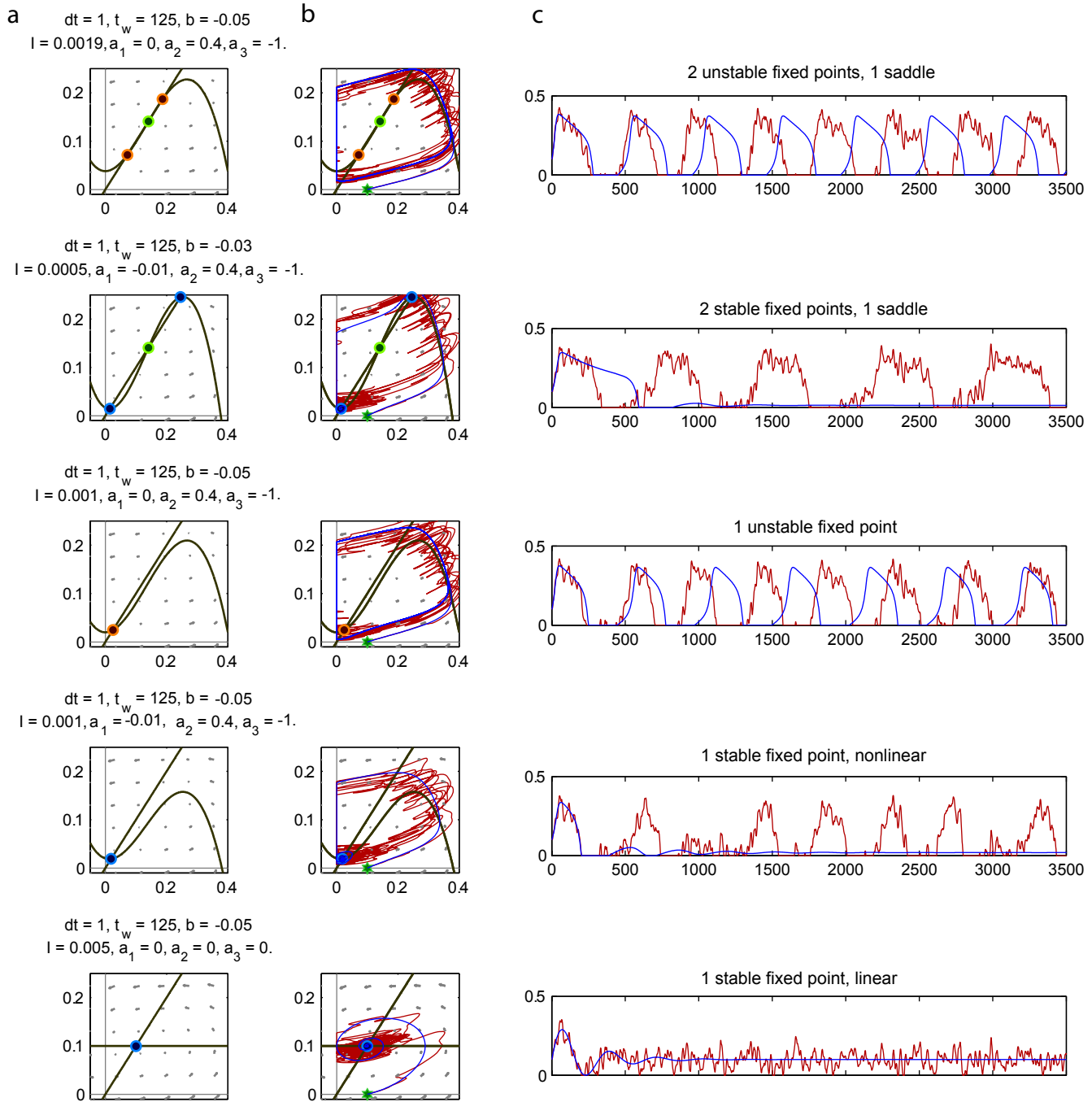




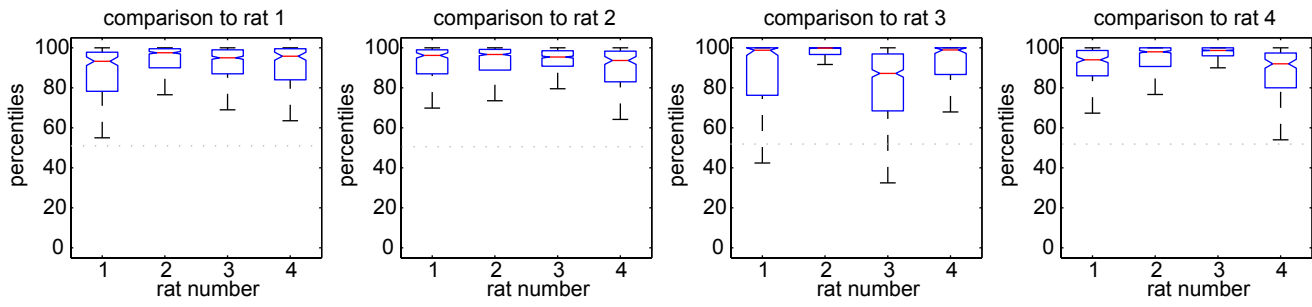




Persistent response vs. past activity (computed for different values of tau) on phantom control trials for rat 1.



used activity state and dynamic state from comparison trials



used dynamic state only from comparison trials, kept original activity state

